Article

Analysis and Design of the Energy Storage Requirement of Hybrid Modular Multilevel Converters Using Numerical Integration and Iterative Solution

Kailun Wang [1] , **Qiang Song** [1,*] **and Shukai Xu** [2]

[1] Department of Electrical Engineering, Tsinghua University, Beijing 100084, China;
wkl20@mails.tsinghua.edu.cn
[2] Electric Power Research Institute of China Southern Power Grid, Guangzhou 510663, China; xusk@csg.cn
*   Correspondence: songqiang@tsinghua.edu.cn

Abstract: Increasing the modulation index by utilizing the negative voltage states of full-bridge submodules (FBSMs) can greatly reduce capacitor usage of modular multilevel converters (MMCs), thereby optimizing the cost and volume. The hybrid MMC is composed of half-bridge submodules (HBSMs) and FBSMs, and the capacitor voltages of the two types of submodules (SMs) have different shapes as long as negative voltage states exist. This condition greatly complicates the analysis and design of the energy storage requirement of the hybrid MMC, which utilizes the negative voltage states of FBSMs to boost the AC voltage. A numerical calculation method for solving the capacitor voltages and designing the capacitances of FBSMs and HBSMs is proposed in order to accurately determine the minimum energy storage requirement considering the difference between the energy variations in FBSMs and HBSMs. In the numerical calculation, the energy storage and voltage of the arm are decomposed into FBSM and HBSM parts. According to the physical switching process, the output voltages of FBSM and HBSM parts are determined separately. The one-cycle waveforms of the capacitor voltages are then obtained by numerical integration of the power flows in FBSM and HBSM parts. An iterative solution procedure and the termination criterion that can ensure the accuracy of the obtained one-cycle waveforms are also proposed. Using the numerical integration and iterative solution procedure as the kernel algorithm, the proposed method can accurately analyze the capacitor voltages of the FBSMs and HBSMs and determine the minimum energy storage requirement of the hybrid MMC. Furthermore, the proposed method is applicable for various operating working conditions and various proportions of FBSMs. The simulation results verify the feasibility and accuracy of the analysis and design method.

Keywords: hybrid modular multilevel converter; capacitor voltage ripple; capacitor usage

1. Introduction

Modular multilevel converters (MMCs) have been widely used in voltage-source-converter-based high-voltage direct-current (VSC-HVDC) transmission. Compared with the two- or three-level converters, MMCs have a modular structure and can achieve higher output voltages with lower harmonics and losses [1–5]. Each submodule (SM) has a large capacitor to maintain the capacitor voltages and limit the capacitor voltage ripple within an acceptable level. However, because a large energy variation in each arm of an MMC exists, the required SM capacitance is relatively large. In each SM, the capacitor may account for approximately 30% of the cost and 50% of the volume [6], resulting in a cost and volume problem for the MMC. Thus, reducing capacitor usage has become a research focus.

Existing studies generally consider two technical routes to reduce the SM capacitance. The first route reduces the energy variation in the arm through circulating current injection [7–10]. However, the capacitance reduction effect is limited because the injected circulating current also increases the root-mean-square (RMS) and peak values of the arm

current, which reduces the safe operating margin [9,10]. The other route increases the modulation index of the MMC to a higher value. Previous studies have found that this method can greatly reduce both the capacitor usage and the rated AC current simultaneously [11–18]. For example, literature [11] found that the fundamental-frequency capacitor ripple can be eliminated by increasing the modulation index to 1.414 under a pure active power condition, greatly reducing the required capacitance. Literature [12,13] considered the influence of reactive power on the fundamental-frequency capacitor ripple and the double-frequency ripple. In addition, some studies combined the approach of increasing the modulation index with a double-frequency circulating current injection, third harmonic voltage injection, and other methods to further reduce the capacitor voltage ripple and capacitor usage [14–18].

The half-bridge submodule (HBSMs)-based MMC (HB-MMC) is the most commonly used topology. However, the maximum attainable modulation index of the HB-MMC is limited. To increase the modulation index to such a high value that the energy variation and energy storage requirement can be reduced, an MMC composed of FBSMs (FB-MMC) is used. The capacitor voltage ripple and the required SM capacitance can be obtained through the overall energy stored in the arm, which can be obtained by integrating the power flow in the arm. The analysis approach of the overall arm energy, which is based on the assumption that all of the SMs in each arm equally share the stored energy all the time, is only applicable to an FB-MMC that contains only one type of SM. However, the semiconductor usage of the FB-MMC is extremely high, and the resulting cost and volume of the MMC are even larger than those of a conventional MMC, even if the energy storage requirement is minimized by increasing the modulation index.

Another approach is adding several extra full-bridge SMs (FBSMs) in each arm (utilizing their negative voltage states) to the conventional HB-MMC to form a hybrid MMC [19], which can lower the increase in semiconductor usage. In this scenario, the rated DC voltage remains unchanged, and the rated AC voltage and modulation index can be increased linearly with the increase in FBSMs. However, exactly evaluating and designing the energy storage requirement of a hybrid MMC that utilizes negative voltage states is greatly challenging. The hybrid MMC contains FBSMs and HBSMs in each arm and the energy variation and the capacitor voltages of the two types of SMs are significantly different if the arm voltage has a period of negative states [20–22]. This condition is mainly because only the FBSMs are charged or discharged, whereas all of the HBSMs are bypassed during the negative-voltage period. Therefore, the shape of the capacitor voltage ripple and the required SM capacitance of the two types of SMs are relatively different in a hybrid MMC, and the analysis approach through the overall arm energy is inapplicable. Although the reduction effect of the cost and size of hybrid MMC using negative voltage states is analyzed in [13], the difference between the energy storage variation of the two types of SMs is not considered, and the analysis is still based on the overall arm energy—the accuracy of which can only be ensured to the MMCs, whose arms are composed of the same type of SMs. Some research efforts have been conducted on the analysis and design method of the energy storage requirement of hybrid MMCs [14–16]. The accuracy and applicability of these methods for various operating conditions should be further explored because they are based on some assumptions that are only true for some special conditions. The charging and discharging processes of the capacitors in HBSMs and FBSMs are analyzed physically using piecewise analysis in [17]; they are mainly focused on the working condition with a power factor of no less than 0.9 and a proportion of FBSMs equal to 2/3.

In this study, a numerical calculation method for solving the capacitor voltages and designing the capacitances of FBSMs and HBSMs is proposed in order to provide a method that can accurately determine the minimum energy storage requirement, considering the difference between the energy variations in FBSMs and HBSMs. First, the energy storage and voltage of the arm are decomposed into FBSM and HBSM parts, and the output voltage of these parts is determined separately according to the physical switching process. A numerical integration method is then adopted to obtain the one-cycle waveforms of the

capacitor voltages. To solve the problem that the initial values of the capacitor voltages of the FBSMs and HBSMs cannot be exactly determined, an iterative solution procedure and the termination criterion that can ensure the accuracy of the obtained one-cycle waveforms are proposed. Then, based on the numerical integration and iterative solution procedure as the kernel algorithm, the method for finding the minimum energy storage requirement of the hybrid MMC and determining the capacitances of the FBSMs and HBSMs is proposed. The simulation results verify the feasibility and accuracy of the analysis and design method.

2. Hybrid MMC Utilizing Negative Voltage States of FBSMs

Previous studies have found that increasing the modulation index can significantly reduce the capacitor usage of MMCs. However, the arm of the conventional HB-MMC cannot output negative voltage states, so the modulation index is limited to 1.0. To achieve a high modulation index while lowering the increase in semiconductor usage, several extra FBSMs can be appended to each arm of the HB-MMC to form a hybrid MMC. As shown in Figure 1, an HB-MMC with N_0 submodules is appended with F FBSMs to form a hybrid MMC. In Figure 1, phase A is considered for illustration, where u_{ap} and u_{an} are the arm voltages, i_{ap} and i_{an} are the arm currents, and U_{dc} is the DC voltage.
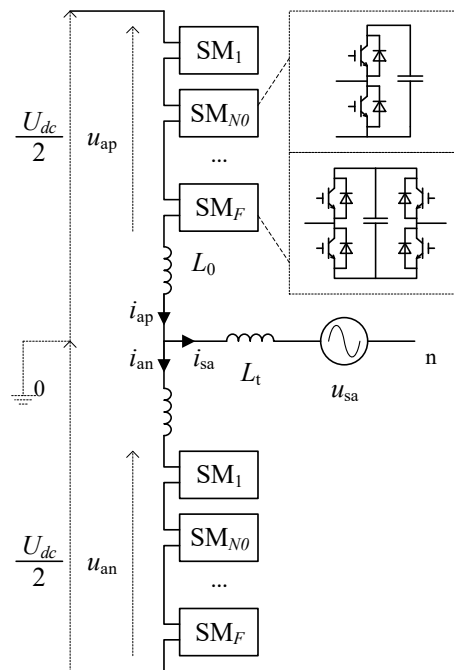

Figure 1. Illustration of the hybrid MMC.

Ignoring the losses, the equivalent circuit of the MMC connected to the AC grid is shown in Figure 2. The AC grid voltage phasor is denoted using $\boldsymbol{U_s} = U_s \angle 0$, where U_s is the rated RMS value of the phase voltage. The phasor of the AC port voltage of the MMC is denoted using $\boldsymbol{U_{ac}} = U_{ac} \angle \delta$. According to the equivalent circuit shown in Figure 2, the phasor of the AC port voltage can be expressed as follows:

$$\boldsymbol{U_{ac}} = \boldsymbol{U_s} + jX\boldsymbol{I_{ac}}, \tag{1}$$

where $\boldsymbol{I_{ac}} = I_{ac} \angle -\varphi$ is the phasor of the output AC current, I_{ac} is the RMS value of the AC current, and φ is the power factor angle. X is the equivalent reactance between the MMC and the AC grid, including the line reactance between the MMC and PCC, transformer leakage reactance, and arm reactance. When outputting the AC current $I_{ac} \angle -\varphi$, the RMS value and phase angle of the AC port voltage of the MMC can be expressed as follows:

$$U_{\text{ac}} = \sqrt{(U_\text{s} + X I_{\text{ac}} \sin \varphi)^2 + (X I_{\text{ac}} \cos \varphi)^2} \tag{2}$$
$$\approx U_\text{s}\left(1 + \frac{X I_{\text{ac}} \sin \varphi}{U_\text{s}}\right),$$

$$\delta = \arctan \frac{X I_{\text{ac}} \cos \varphi}{U_\text{s} + X I_{\text{ac}} \sin \varphi}. \tag{3}$$

Therefore, at the operating point when outputting the AC current $I_{\text{ac}} \angle \text{-} \varphi$, the corresponding modulation index M_{ac} is expressed as follows:

$$M_{\text{ac}} = \frac{\sqrt{2} U_{\text{ac}}}{U_{\text{dc}}/2} = \frac{\sqrt{2}(U_\text{S} + X I_{\text{ac}} \sin \varphi)}{U_{\text{dc}}/2} = M_0(1 + X^* I_{\text{ac}}^* \sin \varphi), \tag{4}$$

where X^* is the per-unit value of the equivalent reactance, I^*_{ac} is the per-unit value of the ac-side current, and M_0 is the base modulation index when the MMC outputs zero current, and is expressed as follows:

$$M_0 = \frac{\sqrt{2} U_\text{S}}{U_{\text{dc}}/2}. \tag{5}$$

The base modulation index M_0 also represents the per-unit AC grid voltage normalized by $U_{\text{dc}}/2$.
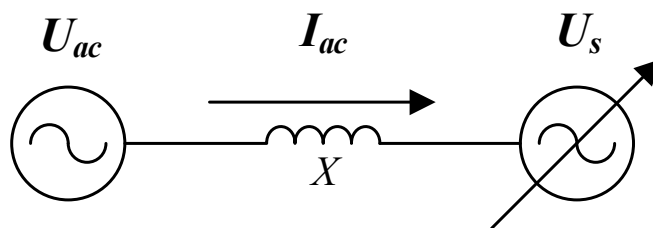

Figure 2. Equivalent circuit of the MMC connected to the AC grid.

Figure 3 shows an example of the relation between the number of extra FBSMs and the MMC arm voltage. The rated voltage of the capacitor is denoted as U_c and can be expressed as follows:

$$U_\text{c} = \frac{U_{\text{dc}}}{N_0}. \tag{6}$$

If the number of the extra FBSMs in each arm is denoted using F, then the range of the arm voltage is $[-FU_\text{c}, N_0 + FU_\text{c}]$. To satisfy the linear modulation constraint, the peak and valley values of the arm voltages at any operating point should be within the range $[-FU_\text{c}, N_0 + FU_\text{c}]$, which can be expressed as follows:

$$\begin{cases} \frac{M_{\text{ac}}+1}{2} U_{\text{dc}} < (N_0 + F) U_\text{c}, \\ -FU_\text{c} > \frac{1 - M_{\text{ac}}}{2} U_{\text{dc}}. \end{cases} \tag{7}$$

According to Equation (7), the number of extra FBSMs should satisfy the following condition:

$$\frac{F}{N_0} > \frac{M_{\text{ac}} - 1}{2}. \tag{8}$$
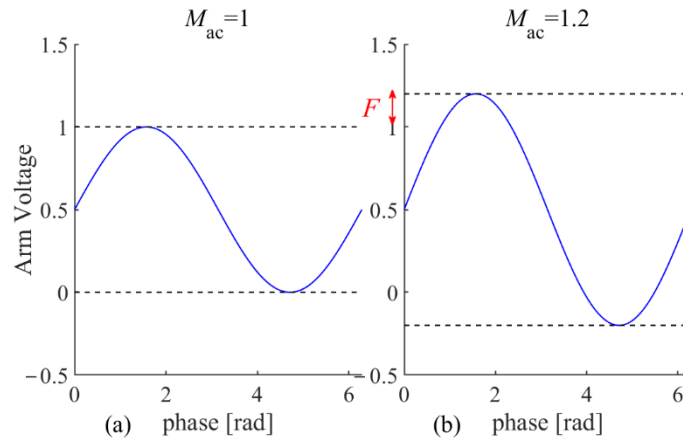
Figure 3. Relation between the number of FBSMs and the arm voltage: (**a**) HB-MMC; (**b**) hybrid MMC.

Evidently, the maximum modulation index of all possible operating points determines the minimum required number of extra FBSMs. The operating range of MMC can be described using the PQ diagram, as shown in Figure 4. The main function of the MMC in the VSC-HVDC system is to transfer the active power. Existing studies have demonstrated that the capacitor voltage ripple under a high capacitive power condition is much greater than a pure active power condition. Outputting a reactive power of rated capacity in actual applications is not required, and a maximum reactive power requirement, which is denoted using $\pm Q_{max}$, is usually set according to the requirement of the connected AC grid. Therefore, the operating region of the MMC is shown as the shaded area in Figure 4. According to Equation (4), the maximum modulation index within the given operating region can be expressed as follows:

$$M_{ac\_max} \approx M_0(1 + X^* Q_{max}), \tag{9}$$

where the maximum modulation index is related to M_0 and Q_{max} given that the value of X^* is certain. Then, combining Equations (8) and (9), the required minimum number of the extra FBSMs is determined by the base modulation index and maximum reactive power requirement, as follows:

$$F_{min} = \frac{M_{ac\_max} - 1}{2} N_0. \tag{10}$$
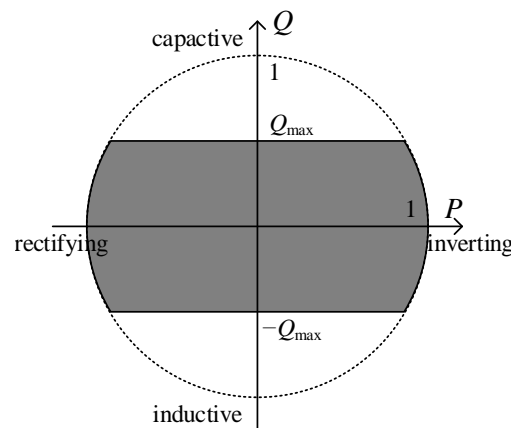
Figure 4. P/Q operating region of MMC considering maximum reactive power requirement.

3. Algorithm for Solving the One-Cycle Waveforms of the Capacitor Voltages of FBSMs and HBSMs

The peak values of the capacitor voltages for a certain operating point should be exactly calculated, because the capacitances of the SMs should be designed to satisfy the constraint that the peak values of the capacitor voltages be below the permitted upper limit under all possible operating conditions. A physical switching process-based numerical calculation method for solving the one-cycle waveforms of the capacitor voltage is proposed: The energy storage and voltage of the arm are decomposed into FBSM and HBSM parts, and the output voltages of these parts are determined separately according to the actual switching process; then, a numerical integration and iterative solution procedure are proposed to obtain the accurate one-cycle waveforms of the capacitor voltages of the FBSMs and FBSMs. The obtained accurate one-cycle waveforms can be used to determine the peak values of the capacitor voltages of the FBSMs and HBSMs and further provide a base for finding the minimum capacitor usage of the hybrid MMC.

3.1. Arm Energy and Voltage Decomposition for Hybrid MMC

For the hybrid MMC, the capacitor voltages of the HBSMs and FBSMs should be calculated separately. The capacitor voltage sorting algorithm is assumed to achieve a good balance among all the FMSMs and among all the HBSMs. Therefore, the FBSM capacitor voltages can be denoted using a single variable $u_{cf}(t)$, and the HBSM capacitor voltages can be denoted using a single variable $u_{ch}(t)$. The capacitor voltages of $u_{cf}(t)$ and $u_{ch}(t)$ may not be equal; thus, directly solving the capacitor voltage through the overall stored energy in each arm is impossible. However, the energy stored in each arm can be decomposed into two parts of FBSMs and HBSMs. For each part, the same relation between stored energy and the capacitor voltages still holds.

The required capacitance of the FBSMs and HBSMs is also different because the FBSMs and HBSMs in a hybrid MMC have different energy variations. The HBSM capacitance is denoted as C_d. The ratio of the capacitance of the FBSMs to that of the HBSMs is the capacitance ratio k_f, and the FBSM capacitance is $k_f C_d$. Under the operating conditions when the modulation index is greater than 1.0, the capacitor voltages of the FBSMs fluctuate greater than those of the HBSMs, thereby increasing the total capacitor usage requirement. By appropriately increasing the capacitance ratio, the voltage ripple of the FBSMs can be reduced to decrease the overall capacitor usage of the MMC. The calculation method considers this factor.

The instantaneous energy stored in each arm can then also be decomposed into FBSM and HBSM parts, expressed as follows:

$$\begin{cases} e_f\left(t\right) = F\frac{1}{2}(k_f C_d)u_{ch}^2(t), \\ e_h\left(t\right) = N_0\frac{1}{2}(C_d)u_{cf}^2(t). \end{cases} \tag{11}$$

The capacitor usage can also be represented using the energy storage requirement E_{nom}, which is defined as the normalized energy that is stored in all of the SM capacitors when the SM capacitor voltage is its nominal value [11,12]. In hybrid MMCs, the total energy storage requirement can be decomposed into the energy storage requirements of FBSMs and HBSMs, which are denoted as E_{nomf} and E_{nomh}, respectively, as follows:

$$\begin{cases} E_{nomf} = \frac{6 \times \frac{1}{2}(k_f C_d)F U_c^2}{S_N} = \frac{k_f F}{1+k_f F}E_{nom}, \\ E_{nomh} = \frac{6 \times \frac{1}{2}C_d N_0 U_c^2}{S_N} = \frac{1}{1+k_f F}E_{nom}, \end{cases} \tag{12}$$

where S_N is the rated capacity of the MMC, and E_{nom} is the total energy storage requirement, which can be expressed as follows:

$$E_{nom} = E_{nomf} + E_{nomh}. \tag{13}$$

To calculate the capacitor usage of the FBSM and HBSM parts, the arm voltages should also be decomposed into two parts, whose voltages can be determined according to the sorting algorithm. The commonly used sorting algorithm is shown in Figure 5. The output voltages of the FBSM and HBSM parts can be obtained according to the relation among arm voltage, arm current, capacitor voltages, and the number of inserted SMs.

Using the upper arm voltage of phase A as an example, the arm voltage and current can be expressed as follows:

$$u_{\mathrm{arm}}(t) = \frac{U_{\mathrm{dc}}}{2} - \sqrt{2}U_{\mathrm{ac}}\sin(\omega t + \delta), \tag{14}$$

$$i_{\mathrm{arm}}(t) = \frac{1}{3}I_{\mathrm{dc}} + \frac{\sqrt{2}}{2}I_{\mathrm{ac}}\sin(\omega t - \varphi), \tag{15}$$

where I_{dc} is the DC current of the MMC. According to the active power balance between the AC and DC sides of the MMC, the DC current of the MMC can be expressed by AC current as follows:

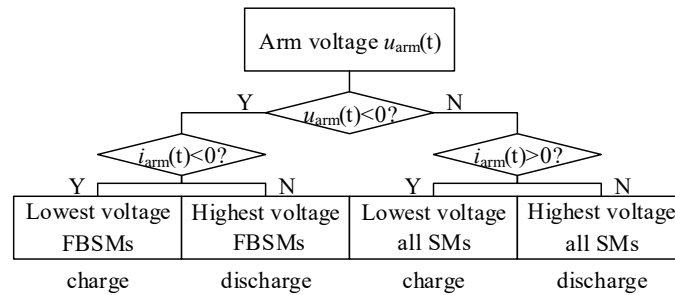$$I_{\mathrm{dc}} = \frac{3}{2\sqrt{2}}M_0 I_{\mathrm{ac}}\cos(\varphi). \tag{16}$$

**Figure 5.** Flowchart of the sorting algorithm.

Figure 6 shows an example of the variation process of the instantaneous capacitor voltages in one fundamental-frequency cycle when the MMC operates under a pure active absorption condition. The negative zero-crossing point of the arm voltage is selected as the origin of the time axis. According to the zero-crossing point of the arm voltage and current, the energy variation of the arm in a fundamental-frequency cycle can be divided into four phases:

(1) Phase 1 (charge)

In this phase, the arm voltage is negative, and only FBSMs participate in voltage output. Therefore, the voltages of the FBSM and HBSM parts can be expressed as follows:

$$\begin{cases} u_{\mathrm{f}}(t) = u_{\mathrm{arm}}(t), \\ u_{\mathrm{h}}(t) = 0. \end{cases} \tag{17}$$

According to nearest-level modulation (NLM), the actual number of the inserted SMs is consistent with the arm voltage. Figure 6d shows the insertion indices of FBSMs and HBSMs. In this phase, only FBSMs are inserted and HBSMs are bypassed. As shown in Figure 6a, the capacitor voltages of the FBSMs increasingly diverge from those of the HBSMs, and reach a peak at the end of this phase because only the FBSMs are charged in this phase.
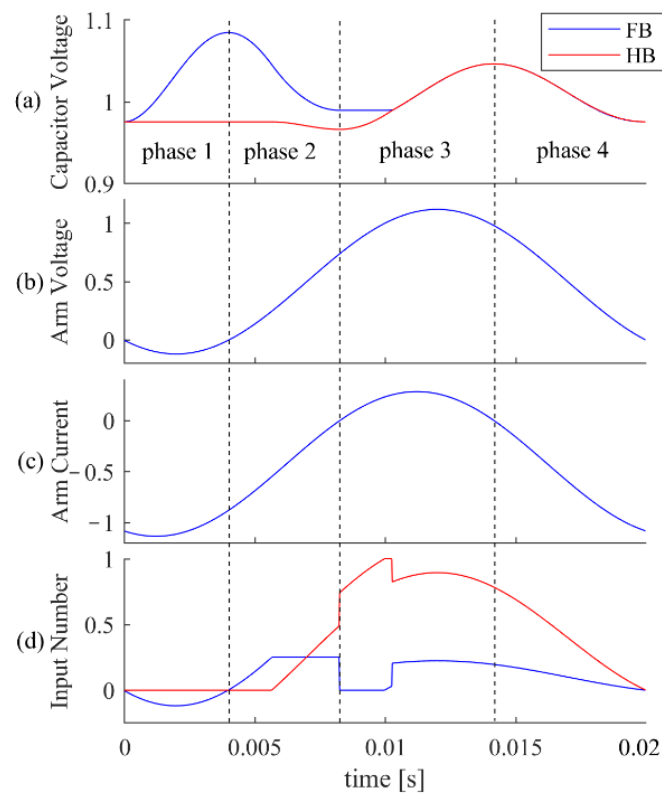
Figure 6. Illustration of capacitor voltage variation process: (**a**) capacitor voltages; (**b**) arm voltage; (**c**) arm current; (**d**) input submodule number.

(2)   Phase 2 (discharge)

The arm voltage becomes positive and the arm current is negative. As a result, the capacitors are discharged in this phase. According to Figure 6a, the capacitor voltages of FBSMs are greater than those of the HBSMs at the beginning of the second phase due to the first charging phase. Therefore, in this phase, the switching strategy initially inserts as many FBSMs as possible under the constraints that the insertion index of FBSMs does not exceed F to discharge their capacitor voltages. The HBSMs then output the remaining arm voltage correspondingly. The voltages of the FBSM and HBSM parts in this phase are expressed as follows:

$$\begin{cases} u_f(t) = \min(u_{arm}(t), FU_c), \\ u_h(t) = u_{arm}(t) - u_f(t). \end{cases} \tag{18}$$

As shown in Figure 6d, the insertion index of FBSMs in the first half of the second phase gradually increases with the demand for arm voltage and finally saturates to F; the remaining arm voltage is generated by HBSMs. As shown in Figure 6a, the capacitor voltages of the FBSMs and HBSMs start to converge gradually in this phase.

(3)   Phase 3 (charge)

In this phase, the arm voltage and current are positive, and the capacitors are charged in this phase. As shown in Figure 6a, at the beginning of this phase, as many HBSMs as possible should be initially inserted when the capacitor voltages of FBSMs are still higher than those of the HBSMs. The voltages of the FBSM and HBSM parts in this phase are expressed as follows:

$$\begin{cases} u_h(t) = \min(u_{arm}(t), N_0 U_c), \\ u_f(t) = u - u_h(t). \end{cases} \tag{19}$$

Subsequently, the capacitor voltages of the FBSMs and HBSMs are equal. At this time, the arm-switching strategy balances the two capacitor voltages. To maintain equal

capacitor voltages, the energy absorbed by the FBSMs and HBSMs should be proportional to their nominal energy storage. The output voltages of the FBSM and HBSM parts should be proportional to their nominal energy storages because the current flowing through the arm is equal, as follows:

$$
\begin{cases}
u_\mathrm{f}(t) = \frac{E_\mathrm{nomf}}{E_\mathrm{nom}} u_\mathrm{arm}(t), \\
u_\mathrm{h}(t) = \frac{E_\mathrm{nomh}}{E_\mathrm{nom}} u_\mathrm{arm}(t).
\end{cases}
\tag{20}
$$

As shown in Figure 6d, in the first half of the third phase, as many HBSMs are inserted as possible. In the second half, the insertion indices of FBSMs and HBSMs are proportional.

(4)   Phase 4 (discharge)

In this phase, the arm voltage is positive and the current is negative, resulting in discharging the capacitors. The same relation of (20) exists because the capacitor voltages of the FBSMs and HBSMs are equal.

This analysis is based on the example of pure active absorption condition. However, the proposed method is not limited to this circumstance. In general, the voltages of FBSM and HBSM parts based on the switching process are summarized in Table 1.

Table 1. Relation between arm voltages of FBSMs and HBSMs.

$u_\mathrm{arm} < 0$		$u_\mathrm{arm} > 0$	
		$i_\mathrm{arm} > 0$	$i_\mathrm{arm} < 0$
Only FBSM input: $u_\mathrm{f} = u_\mathrm{arm}$ $u_\mathrm{h} = 0$	$u_\mathrm{cf} > u_\mathrm{ch}$	Maximum HBSM input: $u_\mathrm{h} = \min(u_\mathrm{arm},\, N_0 U_\mathrm{c})$ $u_\mathrm{f} = u_\mathrm{arm} - u_h$	Maximum FBSM input.
	$u_\mathrm{cf} = u_\mathrm{ch}$	Equally input: $u_\mathrm{f} = \frac{E_\mathrm{nomf}}{E_\mathrm{nom}} u_\mathrm{arm}$ $u_\mathrm{h} = \frac{E_\mathrm{nomh}}{E_\mathrm{nom}} u_\mathrm{arm}$	Equally input.
	$u_\mathrm{cf} < u_\mathrm{ch}$	Maximum FBSM input: $u_\mathrm{f} = \min(u_\mathrm{arm},\, F U_\mathrm{c})$ $u_\mathrm{h} = u_\mathrm{arm} - u_\mathrm{f}$	Maximum HBSM input.

After obtaining the output voltages of the FBSM and HBSM parts, the instantaneous power flowing into the two parts can be obtained by the product of the arm current with the respective voltages of the two parts, as follows:

$$
\begin{cases}
p_\mathrm{f}(t) = u_\mathrm{f}(t) i_\mathrm{arm}(t), \\
p_\mathrm{h}(t) = u_\mathrm{h}(t) i_\mathrm{arm}(t).
\end{cases}
\tag{21}
$$

The instantaneous energy stored in the FBSM and HBSM parts can then also be expressed by integrating the corresponding instantaneous power, as follows:

$$
\begin{cases}
e_\mathrm{f} = \int p_\mathrm{f} dt = \int u_\mathrm{f}(t) i_\mathrm{arm}(t), \\
e_\mathrm{h} = \int p_\mathrm{h} dt = \int u_\mathrm{h}(t) i_\mathrm{arm}(t).
\end{cases}
\tag{22}
$$

Referring to Equation (11), the capacitor voltages (p.u.) of the FBSM and HBSM parts can then be calculated as follows:

$$
\begin{cases}
u_\mathrm{cf}^*(t) = \sqrt{\frac{6 e_\mathrm{f}(t)}{S_\mathrm{N} E_\mathrm{nomf}}}, \\
u_\mathrm{ch}^*(t) = \sqrt{\frac{6 e_\mathrm{h}(t)}{S_\mathrm{N} E_\mathrm{nomh}}}.
\end{cases}
\tag{23}
$$

3.2. Numerical Integration and Iterative Solution Procedure

Based on the decomposed arm energy and voltage, a numerical integration and iterative solution procedure is proposed. The numerical calculation aims to obtain the one-

cycle waveforms of the capacitor voltages under a certain operating condition and thereby obtains the peak values of the capacitor voltages for capacitance design. The flowchart of the numerical integration and iterative solution procedure is shown in Figure 7. The detailed descriptions of the main steps of the numerical calculation process for obtaining the one-cycle waveforms are as follows:

(1) Initial values of the numerical calculation.

The initial values should be set for the numerical calculation. As analyzed in Section 3.1, the numerical calculation starts at the negative zero-crossing point of the arm voltage. From the view of the overall energy, if the initial value of the overall energy is set as $e(0)$, then the energy stored in the overall arm can be expressed as follows:

$$e(t) = e(0) + \int_0^t u_{\text{arm}}(\tau) i_{\text{arm}}(\tau) \mathrm{d}\tau. \tag{24}$$

Note that the Volterra operator is adopted, which has also gained applications for storage system modeling and control [23]. Under steady-state operation, the average value of the overall arm energy storage in one fundamental-frequency cycle should be the nominal energy storage, and the following equation can be obtained:

$$\frac{1}{T_1} \int_0^{T_1} e(t) \mathrm{d}t = e(0) + \frac{1}{T_1} \int_0^{T_1} \left(\int_0^t u_{\text{arm}}(\tau) i_{\text{arm}}(\tau) \mathrm{d}\tau \right) \mathrm{d}t = \frac{S_N E_{\text{nom}}}{6}, \tag{25}$$

where T_1 is the fundamental-frequency period. Therefore, the initial value of the overall arm energy can be determined as follows:

$$e(0) = \frac{S_N E_{\text{nom}}}{6} - \frac{1}{T_1} \int_0^{T_1} \left(\int_0^t u_{\text{arm}}(\tau) i_{\text{arm}}(\tau) \mathrm{d}\tau \right) \mathrm{d}t. \tag{26}$$

The initial value of the overall arm energy can be determined in advance of the numerical calculation because the arm voltage and current can be determined as shown in (14) and (15) in advance.

However, the numerical calculation needs the initial values of the capacitor voltages of the FBSMs and HBSMs. Considering that the ripple component is related to the power factor angle of the operating point, the values of the first time point of the one-cycle waveforms of the capacitor voltages are generally not equal to the DC rated value. Furthermore, the values of the first time point of the capacitor voltages of the HBSMs and FBSMs may be different. This condition brings great difficulties in determining the initial values of the capacitor voltages. To start the numerical calculation, the initial values of the capacitor voltages of FBSMs and HBSMs are assumed to be equal and are determined by the initial overall arm energy, as follows:

$$u_{\text{cf}}^*(0) = u_{\text{ch}}^*(0) = \sqrt{\frac{6e(0)}{S_N E_{\text{nom}}}} \tag{27}$$

This assumption only aims to initiate the numerical calculation, and it does not indicate that the values of the first time points of the capacitor voltages of FBSMs and HBSMs always appear equal in the numerical calculation. The values of the first time points of the one-cycle waveforms are corrected iteratively in step (3).

(2) Numerical integration to obtain temporary one-cycle waveform.

For a certain operating point, the arm voltage and current can be calculated, as shown in Equations (14) and (15). According to the analysis in Section 3.2, the output voltages of the FBSM and HBSM parts can be determined referring to Table 1. The discretized

instantaneous power of the two parts at the *k*-th time-step point can then be obtained as follows:

$$\begin{cases} p_{\text{f}}(k) = u_{\text{f}}(k)i_{\text{arm}}(k), \\ p_{\text{h}}(k) = u_{\text{h}}(k)i_{\text{arm}}(k). \end{cases} \tag{28}$$

The energy storages of the FBSM and HBSM parts at the next time-step point can be obtained through numerical integration of the respective instantaneous power. A left-hand rectangle integration formula is adopted for its simplicity and accuracy in small time steps. It satisfies

$$\begin{cases} e_{\text{f}}(k+1) = e_{\text{f}}(k) + p_{\text{f}}(k)\Delta t, \\ e_{\text{h}}(k+1) = e_{\text{h}}(k) + p_{\text{h}}(k)\Delta t, \end{cases} \tag{29}$$

where Δt is the time-step of the numerical calculation. According to the relationship between the energy storage and capacitor voltage, the capacitor voltages of the FBSM and HBSM parts at the next time-step point can be expressed as follows:

$$\begin{cases} u_{\text{cf}}(k+1) = \sqrt{\dfrac{6e_{\text{f}}(k+1)}{S_{\text{N}}E_{\text{nom f}}}}, \\ u_{\text{ch}}(k+1) = \sqrt{\dfrac{6e_{\text{h}}(k+1)}{S_{\text{N}}E_{\text{nom h}}}}. \end{cases} \tag{30}$$

The calculation for the next time step point is then performed until the calculation of a fundamental-frequency period is completed and the temporary one-cycle waveforms of the capacitor voltages are obtained.

(3)   Iterative solution procedure for obtaining the final one-cycle waveforms.

At step (1), the initial voltages of the FBSM and HBSM parts are assumed to be equal, which may be not true when the capacitance ratio of FBSMs and HBSMs is not 1. As a result, a single calculation using step (2) cannot guarantee the accuracy of the obtained one-cycle waveforms of the capacitor voltages. To guarantee accuracy, an iterative solution procedure is proposed to obtain the final accurate one-cycle waveforms. In the iterative solution procedure, the calculation for solving one-cycle waveforms in step (2) is performed iteratively, and the values of the final time-step point of the obtained one-cycle waveforms are used as the initial values of the next iterative calculation. Based on the physical process of capacitor voltage balancing which drives the capacitor voltages of FBSMs and HBSMs equal, the values of the first and final time-step points of the accurate one-cycle waveforms will converge because the waveforms of the capacitor voltages are periodic. Therefore, the termination criterion of the iterative solution procedure is that the relative error between the values of the first and final time-step points of the obtained one-cycle waveforms is less than a preset tolerance. Moreover, it must be mentioned that the convergence of capacitor voltages of the hybrid MMC is related to the hybrid ratio (F/N_0), modulation index, and AC power factor [20]. As the main focus of this paper is the calculation method of capacitor voltages and energy storage design of hybrid MMCs, detailed convergence analysis is omitted.

Note that a very low tolerance will increase iteration time, as the capacitor voltage needs many cycles to converge under this tolerance. On the contrary, a high tolerance will cause inaccurate results, as the capacitor voltages may not reach steady states. Thus, a moderate tolerance of 0.1% is set in order to balance the accuracy and speed in this paper. The 0.1% tolerance is relatively accurate, as it is much lower than the 10% capacitor voltage ripple to be calculated. On the other hand, the iteration process only takes a few cycles under the 0.1% tolerance in our calculation, which improves the calculation's efficiency. Using the iterative solution procedure, the final accurate one-cycle waveforms of the capacitor voltages can be obtained after a few iterations.
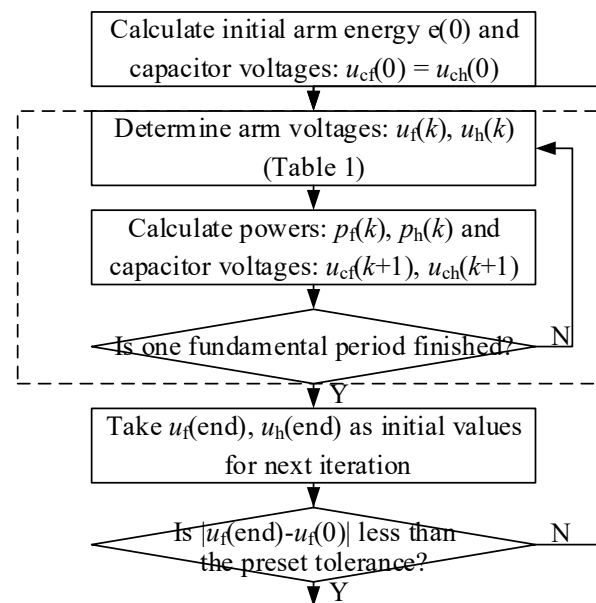
Figure 7. Computing process of capacitor voltages.

4. Method for Finding the Minimum Required Capacitances

The capacitances of the FBSMs and HBSMs should be selected to ensure that the peak values of the capacitor voltages of the FBSMs and HBSMs are below the permitted upper limit under all possible points. To minimize the cost and volume, the minimum capacitor usage (energy storage requirement) and the respective capacitances of the FBSMs and HBSMs that can satisfy this constraint should be determined. For a certain operating point and a certain set of parameters, the peak value of the capacitor voltages can be determined according to the obtained one-cycle waveforms. Therefore, using the numerical integration and iterated solution procedure presented in Section 3 as the kernel algorithm, a method for finding the minimum capacitor usage and the respective capacitances of the FBSMs and FBSMs is proposed.

Prior to finding the minimum required capacitor usage, the base modulation index M_0, the P/Q range, and the permitted upper limit of the capacitor voltage ε_{lim}, which are the key factors that affect the energy variation and capacitor usage of the MMC, should be specified initially. The maximum reactive power Q_{max} can be specified, and the P/Q range is depicted as the shaded area in Figure 4.

One of the complexities of the hybrid MMC is that the capacitances of the FBSMs and HBSMs may not be equal. Therefore, the total capacitor usage E_{nom} and the capacitance ratio k_f should be considered the search variables. Figure 8 shows the flowchart to find the minimum capacitor usage for a certain configuration (M_0 and P/Q range). The searching algorithm includes outer and inner loops. The outer-loop variable is the capacitance ratio k_f. A reasonable range of k_f, such as [1.0, 4.0], can be set for the outer-loop search. For each value of k_f, the maximum value of E_{nom_i} that allows all operating points within the given P/Q range to satisfy the constraint of peak values of the capacitor voltages is found using the dichotomy method. Finally, all the obtained values of E_{nom_kf} are compared, and the minimum value is selected as the final capacitor usage E_{nom}; the corresponding capacitance ratio k_f is also determined. According to Equations (12) and (13), the energy storage requirements and capacitances of the FBSMs and HBSMs are also determined.

The curves of the energy storage requirement with the change in M_0 and Q_{max} can also be obtained by varying the values of M_0 and Q_{max}.
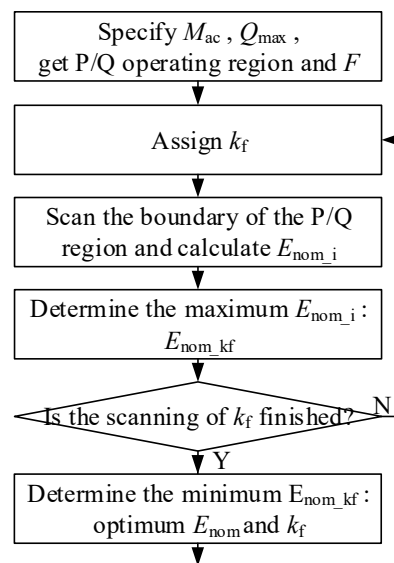
Figure 8. Computing process of capacitor usage and FBSM quantity.

5. Case Study and Simulation

To verify the accuracy of the proposed numerical calculation method, an electromagnetic simulation model of a hybrid MMC was built in MATLAB/Simulink, where all parts of the simulation model were kept consistent with the real application, e.g., main circuit topology and parameters, converter control, pulse generation, capacitor voltage balancing, etc. As shown in Figure 9, the AC side of the hybrid MMC is connected with an AC grid, and the DC side is connected with a DC current source. The hybrid MMC operates under the U_{dc}/Q control mode. The DC voltage is controlled as the rated value, and the active power can be adjusted by the DC current. The reactive power is controlled by the MMC. Simulations have been conducted under different scenarios and show high accuracy with the proposed numerical calculation method. Due to the limitation of paper length, only one typical case is considered as an example.
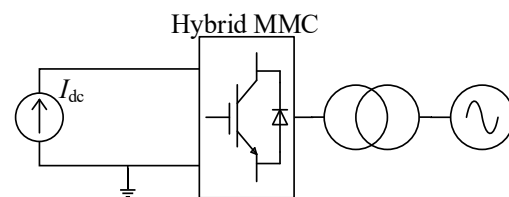

Figure 9. Schematic of the main circuit of the case study.

5.1. Verification of the Theoretical Calculation Algorithm under Certain Values of M_0 and Q_{max}

First, the case of $M_0 = 1.2$ and $Q_{max} = 1.0$ p.u. is considered an example. The permitted upper limit of the capacitor voltage is set to 1.1 p.u. Table 2 lists the obtained parameters using the design method presented in Sections 3 and 4.

The algorithm presented in Section 3 can find the one-cycle waveforms of the capacitor voltages of FBSMs and HBSMs for any given operating points. Figure 10 illustrates the obtained one-cycle waveforms of the capacitor voltages for several typical operating points, such as pure active power input, pure active power output, pure inductive reactive power, and pure capacitive reactive power operating conditions. Consistent with the theoretical analysis, the waveforms of the capacitor voltages of the FBSMs and HBSMs have different shapes as long as negative voltage states exist. The capacitor voltages of the FBSMs and HBSMs can be accurately calculated based on the proposed arm voltage decomposition method and numerical integration and iterative solution procedure. The simulation results are also illustrated in Figure 10. The figure shows that the simulation and

theoretical calculation results fit effectively, thereby verifying the accuracy of the proposed calculation method.

The peak values of the capacitor voltages can be determined according to the obtained one-cycle waveforms. Under the constraint that the peak values of the capacitor voltages of the FBSMs and HBSMs are below the permitted upper limit under all possible points, the minimum capacitor usage and the corresponding capacitances of the FBSMs and FBSMs can be found using the method presented in Section 4. In this case study, when $M_0 = 1.2$, $Q_{max} = 1.0$ p.u. and $\varepsilon_{lim} = 1.1$ p.u., the search result of the minimum energy storage requirement is 35.7 kJ/MVA. Correspondingly, the capacitances of the FBSMs and FBSMs are 18.2 and 14 mF, respectively, and the capacitance ratio k_f is 1.3. In this example, the capacitor voltage ripple under the rated capacitive reactive power condition ($\varphi = \pi/2$) is the highest, because Q_{max} is set to 1.0 p.u. and it is relatively high. As illustrated in Figure 10d, using the designed capacitances, the peak values of the capacitor voltages of the FBSMs and HBSMs are relatively close to 1.1 p.u., which also verifies the feasibility of the method for finding the minimum capacitor usage and the capacitances of the FBSMs and HBSMs.

Table 2. Main parameters of the case study.

Parameters	Values
Rated capacity	1250 MVA
Rated DC voltage	400 kV
Rated AC voltage (line)	294 kV ($M_0 = 1.2$)
Maximum reactive power	1 p.u.
Rated capacitor DC voltage	2 kV
Equivalent AC reactance	44 mH (0.25 p.u.)
HBSM quantity	200 (1 p.u.)
FBSM quantity	50 (0.25 p.u.)
Capacitor usage	35.7 kJ/MVA
Capacitance ratio	1.3
Capacitance of FB/HBSM	18.2/14 mF
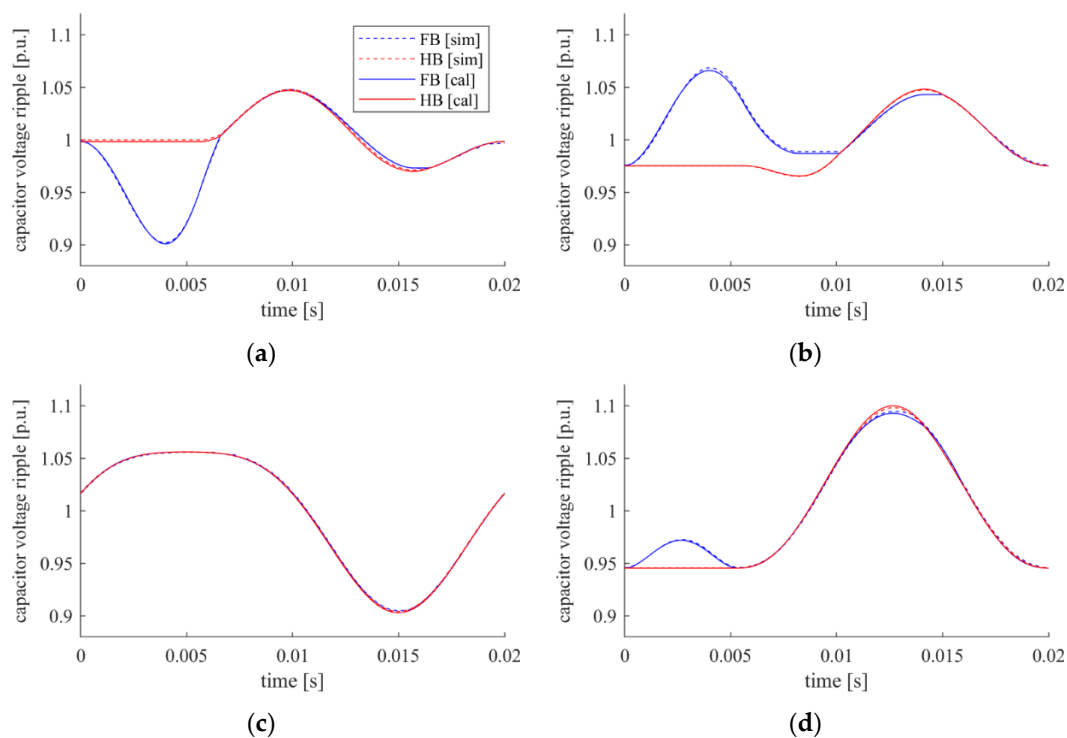
Figure 10. Simulation and calculation waveform of capacitor voltages in different operating points: (**a**) pure active output (inverting) ($\varphi = 0$); (**b**) pure active input (rectifying) ($\varphi = \pi$); (**c**) pure inductive reactive power ($\varphi = -\pi/2$); (**d**) pure capacitive reactive power ($\varphi = \pi/2$).

5.2. Analysis of the Impacts of the Base Modulation Index and Maximum Reactive Power on Capacitor Usage and the Number of Extra FBSMs

The base modulation index M_0, which also represents the normalized rated AC grid voltage, is a key parameter that determines capacitor usage and semiconductor usage. In the existing studies, in which a FB-MMC that only contains FBSMs is considered, the capacitor usage can reach the minimum when the base modulation index is increased to approximately 1.414. However, this conclusion may not be applicable to a hybrid MMC that contains two types of SMs, because determination of the capacitor usage is relatively different from the FB-MMC. The maximum reactive power requirement Q_{max} is another key parameter that affects capacitor usage. Generally, capacitor usage increases with the increase in the maximum reactive power requirement.

For certain values of M_0 and Q_{max}, the minimum required capacitor usage can be found using the method presented in Section 4; then, the impacts of the base modulation index and maximum reactive power on capacitor usage can be observed. Figure 11 shows the curve of the capacitor usage E_{nom}, following the change in the base modulation index M_0. To illustrate the impacts of the maximum reactive power on capacitor usage, three typical cases, namely, $Q_{max} = 1.0$ p.u., $Q_{max} = 0.5$ p.u., and $Q_{max} = 0$ p.u., are shown as examples. In addition, the curves of the capacitor usage of the FB-MMC are shown in Figure 11 for comparison.

Figure 11 shows that increasing M_0 can decrease capacitor usage for the FB-MMC and the hybrid MMC. In addition, decreasing the maximum reactive power requirement can reduce the capacitor usage.

However, Figure 11 also reveals the difference in capacitor usage between the hybrid MMC and the FB-MMC when M_0 is increased further. This concept is overlooked by previous studies when evaluating the cost and volume. As shown in Figure 11, when the value of Q_{max} is large, capacitor usage between the hybrid MMC and FB-MMC is slightly different. However, when the value of Q_{max} is low, capacitor usage of the hybrid MMC starts to increase when M_0 is increased above an inflection point (approximately 1.0), which is much lower than the inflection point (approximately 1.414) of FB-MMC. This finding is caused by the low Q_{max}, where the capacitor usage is determined by the rated active power operating point, and the hybrid MMC has the highest capacitor voltage imbalance under higher M_0. Thus, the capacitor usage of the hybrid MMC is significantly higher than for the FB-MMC. However, when Q_{max} is higher, the capacitor usage is determined by the rated capacitive reactive power operating point because of its inherent large capacitor voltage ripple, even if the capacitor voltage imbalance in the active power operating point is considered. Thus, the capacitor usage in this case differs slightly from the FB-MMC.
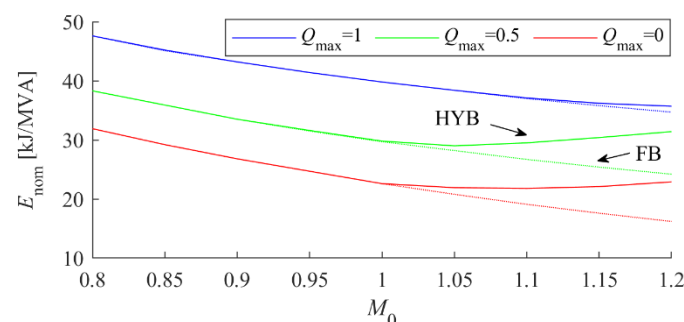

Figure 11. Capacitor usage of hybrid MMC varying with M_0 and Q_{max}.

6. Discussion on Advantages of the Proposed Method and Conclusions

Hybrid modular multilevel converters are a promising choice for future flexible high-voltage DC transmission. In applications of boosted AC voltage or reduced DC voltage, the capacitor voltage of FBSMs and HBSMs differs because of the negative voltage states of FBSMs. It significantly increases the complexity of capacitor voltage ripple calculation and

energy storage design. Several methods have been proposed to solve this problem, and a numerical integration and iterative solution method is proposed in this paper.

Table 3 is listed below to evaluate the above methods qualitatively in three dimensions: accuracy, completeness, and low complexity. Accuracy reflects the simplification degree of the model, i.e., totally neglecting the capacitor voltage difference between FBSMs and FBSMs results in the simplest model but the least accurate; Completeness reflects the application scope of the model, i.e., some calculation methods only consider a limited active power region, a certain hybrid ratio, or a low modulation index. Thus, the model is only applicable in a certain scenario; Low complexity reflects the analytical complexity of the model, i.e., the piecewise calculation method involves considerable discussion and calculation, which is quite complicated in real applications. The comparison table clearly shows the advantages of the proposed method to the previous methods.

Table 3. Comparison table of different methods.

	Accuracy	Completeness	Low Complexity
Arm power calculation [13,16]		●	●
Peak voltage balancing [14]	●		●
Piecewise calculation [19–22]	●		
Detailed piecewise calculation [17]	●	●	
Proposed method	●	●	●

For the proposed method, the energy storage and voltage of the arm are decomposed into FBSM and HBSM parts in the numerical calculation. According to the physical switching process, the output voltage of the FBSM and HBSM parts are described separately. The one-cycle waveforms of the capacitor voltages are then obtained by numerical integration of the power flows in the FBSM and HBSM parts. Furthermore, using the termination criterion, where the relative error between the values of the first and final time-step points of the obtained one-cycle waveforms is less than a preset tolerance, the proposed iterative solution procedure can ensure the accuracy of the final obtained one-cycle waveforms of the capacitor voltages; then, using the numerical integration and iterative solution procedure as the kernel algorithm, the method for finding the minimum capacitor usage and the capacitances of the FBSMs and FBSMs is also proposed. The feasibility and accuracy of the analysis and design method of the energy storage requirement of hybrid MMC are verified using the simulation results.

Nomenclature

N_0	Base number of HBSM.
F	Number of FBSM appended.
u_{ap}	Arm voltage of phase A upper arm.
u_{an}	Arm voltage of phase A lower arm.
i_{ap}	Arm current of phase A upper arm.
i_{an}	Arm current of phase A lower arm.
U_{dc}	DC voltage.
I_{dc}	DC current.
U_s	AC grid RMS phase voltage.
U_{ac}	AC port RMS phase voltage of MMC.
δ	AC port phase voltage phase of MMC.
I_{ac}	AC RMS current of MMC.
φ	AC current phase of MMC.
X	Equivalent reactance between MMC and AC grid.
M_{ac}	Modulation index.
M_0	Base modulation index.
U_c	Base capacitor voltage.
Q_{max}	Maximum reactive power of MMC.
u_{cf}	Capacitor voltage of FBSM.
u_{ch}	Capacitor voltage of HBSM.
C_d	Capacitance of HBSM.
k_f	Capacitance ratio of FBSM to HBSM.
e_f	Arm capacitor energy of FBSM.
e_h	Arm capacitor energy of HBSM.
E_{nom}	Energy storage requirement of MMC.
E_{nomf}	Energy storage requirement of FBSM.
E_{nomh}	Energy storage requirement of HBSM.
S_N	Capacity of MMC.
u_{arm}	Arm voltage.
i_{arm}	Arm current.
u_f	Arm voltage of FBSM.
u_h	Arm voltage of HBSM.
p_f	Arm power of FBSM.
p_h	Arm power of HBSM.
T_1	Fundamental-frequency period.
ε_{lim}	Upper limit of capacitor voltage.
E_{nom_i}	Energy requirement at operating point i.
E_{nom_kf}	Energy requirement at capacitance ratio k_f.
Superscript *	Per unit value.
Functional space	Fundamental-frequency period: $[0, T_1]$.

References

1. Lesnicar, A.; Marquardt, R. An innovative modular multilevel converter topology suitable for a wide power range. In Proceedings of the IEEE Bologna Power Tech Conference Proceedings, Bologna, Italy, 23–26 June 2003; Volume 3, p. 6. [CrossRef]
2. Hagiwara, M.; Akagi, H. Control and Experiment of Pulsewidth-Modulated Modular Multilevel Converters. *IEEE Trans. Power Electron.* **2009**, *24*, 1737–1746. [CrossRef]
3. Tu, Q.; Xu, Z.; Xu, L. Reduced Switching-Frequency Modulation and Circulating Current Suppression for Modular Multilevel Converters. *IEEE Trans. Power Deliv.* **2011**, *26*, 2009–2017.
4. Harnefors, L.; Antonopoulos, A.; Norrga, S.; Angquist, L.; Nee, H.-P. Dynamic Analysis of Modular Multilevel Converters. *IEEE Trans. Ind. Electron.* **2013**, *60*, 2526–2537. [CrossRef]
5. Han, X.; Sima, W.; Yang, M.; Li, L.; Yuan, T.; Si, Y. Transient Characteristics under Ground and Short-Circuit Faults in a ±500 kV MMC-Based HVDC System with Hybrid DC Circuit Breakers. *IEEE Trans. Power Deliv.* **2018**, *33*, 1378–1387. [CrossRef]
6. Davidson, C.; Trainer, D. Innovative concepts for hybrid multi-level converters for HVDC power transmission. In Proceedings of the 9th IET International Conference on AC and DC Power Transmission (ACDC 2010), London, UK, 19–21 October 2010; pp. 1–5.

7. Picas, R.; Pou, J.; Ceballos, S.; Agelidis, V.G.; Saeedifard, M. Minimization of the capacitor voltage fluctuations of a modular multilevel converter by circulating current control. In Proceedings of the IECON 2012—38th Annual Conference on IEEE Industrial Electronics Society, Montreal, QC, Canada, 25–28 October 2012; pp. 4985–4991. [CrossRef]

8. Picas, R.; Pou, J.; Ceballos, S.; Zaragoza, J.; Konstantinou, G.; Agelidis, V.G. Optimal injection of harmonics in circulating currents of modular multilevel converters for capacitor voltage ripple minimization. In Proceedings of the 2013 IEEE ECCE Asia Downunder, Melbourne, Australia, 3–6 June 2013; pp. 318–324.

9. Pou, J.; Ceballos, S.; Konstantinou, G.; Agelidis, V.G.; Picas, R.; Zaragoza, J. Circulating current injection methods based on instantaneous information for the modular multilevel converter. *IEEE Trans. Ind. Electron.* **2015**, *62*, 777–788. [CrossRef]

10. Li, X.; Song, Q.; Liu, W.; Xu, S.; Zhu, Z.; Li, X. Performance Analysis and Optimization of Circulating Current Control for Modular Multilevel Converter. *IEEE Trans. Ind. Electron.* **2016**, *63*, 716–727. [CrossRef]

11. Ilves, K.; Norrga, S.; Nee, H.-P. On energy variations in modular multilevel converters with full-bridge submodules for Ac-Dc and Ac-Ac applications. In Proceedings of the 2013 15th European Conference on Power Electronics and Applications (EPE), Lille, France, 2–6 September 2013; pp. 1–10.

12. Ilves, K.; Norrga, S.; Harnefors, L.; Nee, H.-P. On Energy Storage Requirements in Modular Multilevel Converters. *IEEE Trans. Power Electron.* **2014**, *29*, 77–88. [CrossRef]

13. Song, Q.; Yang, W.; Zhao, B.; Xu, S.; Rao, H.; Zhu, Z. Energy Storage Requirement Reduction Using Negative-Voltage States of a Full-Bridge Modular Multilevel Converter. *IEEE Trans. Power Electron.* **2019**, *34*, 5243–5255. [CrossRef]

14. Judge, P.D.; Chaffey, G.; Merlin, M.M.C.; Clemow, P.R.; Green, T.C. Dimensioning and Modulation Index Selection for the Hybrid Modular Multilevel Converter. *IEEE Trans. Power Electron.* **2017**, *33*, 3837–3851. [CrossRef]

15. Dong, P.; Lyu, J.; Cai, X. Optimized Design and Control for Hybrid MMC With Reduced Capacitance Requirements. *IEEE Access* **2018**, *6*, 51069–51083. [CrossRef]

16. Zhao, C.; Lei, M.; Hu, Y.; Li, Z.; Gao, F.; Wang, P.; Li, Y. Energy Storage Requirement Optimization of Hybrid Modular Multilevel Converter with Circulating Current Injection. *IEEE Trans. Ind. Electron.* **2019**, *66*, 6637–6648. [CrossRef]

17. Lin, L.; Lin, Y.; Xu, C.; Chen, Y. Comprehensive Analysis of Capacitor Voltage Fluctuation and Capacitance Design for Submodules in Hybrid Modular Multilevel Converter with Boosted Modulation Index. *IEEE J. Emerg. Sel. Top. Power Electron.* **2018**, *7*, 2369–2383. [CrossRef]

18. Hu, J.; Xiang, M.; Lin, L.; Lu, M.; Zhu, J.; He, Z. Improved Design and Control of FBSM MMC with Boosted AC Voltage and Reduced DC Capacitance. *IEEE Trans. Ind. Electron.* **2018**, *65*, 1919–1930. [CrossRef]

19. Zeng, R.; Xu, L.; Yao, L.; Williams, B.W. Design and Operation of a Hybrid Modular Multilevel Converter. *IEEE Trans. Power Electron.* **2015**, *30*, 1137–1146. [CrossRef]

20. Lu, M.; Hu, J.; Zeng, R.; Li, W.; Lin, L. Imbalance Mechanism and Balanced Control of Capacitor Voltage for a Hybrid Modular Multilevel Converter. *IEEE Trans. Power Electron.* **2018**, *33*, 5686–5696. [CrossRef]

21. Lu, M.; Hu, J.; Zeng, R.; He, Z. Fundamental-Frequency Reactive Circulating Current Injection for Capacitor Voltage Balancing in Hybrid-MMC HVDC Systems During Riding Through PTG Faults. *IEEE Trans. Power Deliv.* **2018**, *33*, 1348–1357. [CrossRef]

22. Lee, J.-H.; Jung, J.-J.; Sul, S.-K. Balancing of Submodule Capacitor Voltage of Hybrid Modular Multilevel Converter under DC-Bus Voltage Variation of HVDC System. *IEEE Trans. Power Electron.* **2019**, *34*, 10458–10470. [CrossRef]

23. Sidorov, D.; Panasetsky, D.; Tomin, N.; Karamov, D.; Zhukov, A.; Muftahov, I.; Dreglea, A.; Liu, F.; Li, Y. Toward zero-emission hybrid AC/DC power systems with renewable energy sources and storages: A case study from lake Baikal region. *Energies* **2020**, *13*, 1226. [CrossRef]